

Time-Integrated Evidences for Superfluorescence from Magneto-plasmas in Semiconductor Quantum Wells

Y. D. Jho^{1*} and X. Wang², D.H. Reitze^{2,3}, J. Kono⁴, A. A. Belyanin⁵,
V. V. Kocharovskiy^{5,6}, Vl. V. Kocharovskiy⁶, and G. S. Solomon⁷

¹*Department of Information and Communications,*

Gwangju Institute of Science and Technology, Gwangju 500-712, Republic of Korea

²*Department of Physics, University of Florida, Gainesville, Florida 32611, USA*

³*National High Magnetic Field Laboratory, Florida State University, Tallahassee, FL 32310, USA*

⁴*Department of Electrical and Computer Engineering, Rice University, Houston, Texas 77005, USA*

⁵*Department of Physics, Texas A&M University, College Station, Texas 77843, USA*

⁶*Institute of Applied Physics, Russian Academy of Sciences, 603950 Nizhny Novgorod, Russia*

⁷*Solid-State Laboratories, Stanford University, Stanford, California 94305, USA*

We present a comprehensive series of investigations of light emission from semiconductor multiple quantum wells in strong magnetic fields excited by intense femtosecond laser pulses. An analysis of the dependence of the inter-Landau level (LL) emission on magnetic field strength and laser fluence as well as the spatial and statistical characteristics of the emitted light indicate that the initial photo-excited electron-hole pairs spontaneously form a macroscopic coherent state upon relaxation into the LLs, followed by the emission of a superfluorescent burst of radiation. Our results are in good agreement with the predicted characteristics for superfluorescent emission from semiconductor quantum wells. We also investigate the effects of spot size, temperature, excitation geometry, and excitation pulse-width on the emission properties.

PACS numbers: 78.20.Ls, 78.55.-m, 78.67.-n

I. INTRODUCTION

Investigations of coherent phenomena in bulk and quantum-confined semiconductor systems have been made possible in the last fifteen years through the use of ultrafast lasers, which create and probe quantum coherence between electrons and holes on time scales faster than inherent phase-breaking (decoherence) times in these systems, typically 10-100 fs for free carriers to a few picoseconds for excitons. During the coherent temporal regime, the photo-excited carriers retain a well-defined phase relationship with the excitation field, and the induced carrier polarization can be followed as the polarization decays, thus probing fundamental quantum decoherence and scattering. A vast array of ultrafast coherent dynamics in semiconductors has been explored.¹ More specifically, investigations on coherent quantum optics in condensed matter and mesoscopic systems are actively being pursued². In particular, ultrafast semiconductor analogs of quantum optical phenomena such as Rabi flopping³ and superradiance⁴ have been investigated.

An equally important but much less studied phenomenon in semiconductors and nanostructures is the formation of spontaneous macroscopic quantum coherence. Under specific physical conditions, an ensemble of interacting particles can *spontaneously* establish quantum coherence. The spontaneous formation of a coherent quantum ensemble is fundamentally different from laser-driven coherence. Typically, such transitions occur at a critical temperature and/or density at which the particle interactions energetically favor a single N-body wave function. Bose-Einstein condensation (BEC)⁵, super-

conductivity⁶, and superfluidity⁷ are typical examples. While the observation of spontaneous quantum coherence in semiconductors has long been sought after, investigations have been heretofore hampered by the strong electronic interactions and concomitant rapid dephasing times in these systems. Nevertheless, investigations pursuing spontaneous coherence are important because they can reveal much about the underlying fundamental quantum mechanical interactions of N-particle systems. More importantly, they can lead to routes for achieving such sought after goals as BEC in solids. As an example, evidence for a new kind of macroscopic ordered exciton state has been seen in indirect (Type II) quantum wells at sub-Kelvin temperatures excited by ultrafast laser pulses.⁸

Superfluorescence (SF) is a well known example of spontaneously created macroscopic quantum coherence in quantum optics and is a particularly good candidate for these types of investigations. In SF, an incoherently prepared system of inverted two-level atoms develops coherent large amplitude oscillations of the optical polarization starting from the level of quantum fluctuations through the self-phasing process mediated by exchange of photons^{9,10,11}. The resultant macroscopic optical polarization decays superradiantly^{12,13} producing a highly directional burst of coherent radiation. Until now, SF had been observed only in atomic gases^{14,15} and rarefied impurities in crystals^{16,17,18}. Observations of SF emissions from high density systems such as semiconductor electron-hole plasmas have heretofore proven difficult.

We recently reported on the first observation of SF from a dense photo-excited electron-hole plasma in InGaAs/GaAs multiple quantum wells in strong perpendicular magnetic fields¹⁹. Using intense femtosecond

laser pulses to create a dense electron-hole plasma in InGaAs/GaAs multiple quantum wells, combined with a strong perpendicular magnetic field to laterally confine electrons and holes and increase the density of states through Landau quantization, we observed the emission of SF bursts from inter-Landau level (LL) recombination as evidenced from the resulting spectral, spatial, and statistical characteristics of the luminescence. Our investigations revealed a transition from a spontaneous emission (single particle recombination) regime at low carrier densities and magnetic fields through an intermediate (and deterministic) amplified spontaneous emission (ASE) regime to a stochastically emitting SF regime at the highest densities and magnetic fields. In this paper, we present an expanded series of investigations into the time-integrated characteristics of SF emission. We examine how SF is influenced by magnetic field, laser pump pulse fluence, spot size, temperature, and the excitation focal geometry. We also investigate how sublevel mixing influences the emission strength. Finally, we demonstrate that the direction of emission can be efficiently controlled by tailoring the shape of the excitation geometry.

The paper is organized as follows. In Section II, we present the theoretical basis for SF from quantized electron-hole plasmas, present key physical parameters, and discuss the different density- and field-dependent emission regimes. We briefly describe the experimental procedures and details in Section III. Our experimental results are given in Section IV, where we present a comprehensive set of magneto-optical photoluminescence spectra under a variety of relevant conditions. Specifically, we examine the spectral dependence on magnetic field, excitation fluence and duration, excitation geometry, and temperature as well as the spatial characteristics of the emission in different regimes. In addition, analyses of the field scaling and temperature dependence are given. We conclude in Section V.

II. THEORETICAL BACKGROUND

The physics of SF in atomic systems has been studied for more than thirty years; see, e.g., the reviews ^{10,11,20,22,23} and references therein. An incoherently prepared ensemble of excited two level dipoles interacts via the exchange of spontaneously emitted photons. At sufficiently high densities N of inverted atoms, this exchange leads to an effective mutual phasing of the atomic dipole oscillators. As a result, a macroscopic polarization with an amplitude $\propto N$ spontaneously forms arising from quantum fluctuations on a time scale t_d . The resulting polarization decays by emitting a coherent pulse of collective (but spontaneous) radiation with duration t_p scaling as $1/N$ in the simplest case, so that the emitted intensity $I_{SF} \sim N/t_p \sim N^2$ exceeds by many orders of magnitude the intensity I_{SE} of spontaneous emission from the same number of incoherent atoms ($I_{SE} \sim N/T_1 \sim N$). The SF pulse duration t_p and the delay time t_d are *less*

than the times of incoherent spontaneous emission and phase relaxation in the medium: $t_p, t_d < T_1, T_2$. This is a distinctive feature of the phenomenon. In addition, SF is fundamentally a stochastic process: the optical polarization and the electromagnetic field grow from initially incoherent quantum noise to a macroscopic level. Thus, SF is *intrinsically random*: for identical preparation conditions, initial microscopic fluctuations get exponentially amplified and may result in the macroscopic pulse-to-pulse fluctuations in the delay time t_d , electric field polarization, and the direction of the emitted pulse.

We note that there is some terminological confusion in the literature between the two types of cooperative emission processes, superradiance and superfluorescence. Superradiance results when the formation of coherent polarization is driven by an external pump laser field, whereas a superfluorescent macroscopic polarization develops spontaneously due to an intrinsic instability in a system of initially incoherent quantum dipole oscillators. Superradiance is generally easier to observe, and has been previously observed in semiconductors²⁴.

The key to achieving SF is to provide high enough spatial and spectral density of inverted dipole oscillators (atoms, excitons, electron-hole pairs etc.), such that the growth rate of the polarization exceeds the dephasing rate ($1/T_2$). In semiconductors, the rate of the optical polarization decay is typically $1-10 \text{ ps}^{-1}$ or greater, whereas the maximum density of electron-hole pairs within the bandwidth $\Delta\omega$ of the SF pulse is limited by the density of states $\rho(E)$: $N_{max} \sim \rho(E)\hbar\Delta\omega$. It is this combination of a limited gain and fast decoherence that makes it difficult to achieve the threshold for SF^{25,26}. One possible way to overcome these limitations is to use quantum wells placed in strong magnetic fields. The combination of reduced dimensionality and the magnetic field fully quantizes the semiconductor into an atomic-like system with a series of Landau levels (LLs), thus strongly increasing the density of states (DOS)¹⁹. In addition, a complete quantum confinement and filling of all available electron states at the lowest LLs are expected to suppress the dephasing rate of the optical polarization. In our experiments, the initial pumping conditions are chosen so as to ensure the growth of coherence from an incoherent state by exciting the initial e-h plasma high in the bands with an excess energy of 150 meV above the GaAs barrier band gap. The energy difference between the excitation energy and the 0-0 LL in our QWs³⁸ is greater than 270 meV, requiring many scattering events to relax into the QW LLs. The resulting e-h plasma in the individual LLs is thus initially *completely incoherent*.

A. Semiclassical Model of Superfluorescence

To understand the threshold behavior and main features of SF, we will use a coupled density matrix and Maxwell equations in the semiclassical approximation, i.e. assuming a classical electromagnetic field³⁰. Note

that although the optical polarization of an ensemble of quantum oscillators as a whole emerges spontaneously, individual atoms interact with common electromagnetic mode through *stimulated* emission and absorption processes. As the field increases exponentially, semiclassical treatment becomes applicable early in the process and determines its main features. This approach captures the main features of both exponential amplification and subsequent SF pulse formation in various systems¹⁰.

In our experiment, electrons and holes are created by a pumping pulse high in the bands and then quickly lose energy, ending up in the ground subband of QWs before SF starts to develop. We do not consider the initial kinetics of rapid energy and momentum relaxation of carriers with a time scale of 10-500 fs, since these hot carriers do not contribute to SF. We concentrate on carriers that have already reached a quasi-equilibrium degenerate distribution in the lowest LL. We furthermore consider radiation and optical polarization resulting from stimulated optical transitions between electrons and holes on a given LL with the same quantum number. Choosing z as the growth direction, we can write the electric field for y -polarized electromagnetic waves propagating in x -direction as $E_y = (1/2)E_t(y, z)A(x, t)\exp(ikx - i\omega t)$, where E_t is a transverse distribution of the field. It satisfies a 2D Helmholtz equation that determines transverse modes of the structure. For the slowly varying amplitude field A of a given mode and the amplitude polarization P one can obtain

$$\frac{\partial A}{\partial x} + \frac{\mu}{c} \frac{\partial A}{\partial t} + \alpha A = \frac{2\pi i \omega}{\mu c} \Gamma P, \quad (1)$$

$$\frac{\partial \rho_0}{\partial t} = -(\gamma + i\Delta)\rho_0 + i\Omega_R(n_e + n_h - 1), \quad (2)$$

$$\frac{\partial n_e}{\partial t} = \text{Im}[\Omega_R^* \rho_0] + R_e - n_e/T_e(n_e - f_e)/\tau_e, \quad (3)$$

$$\frac{\partial n_h}{\partial t} = \text{Im}[\Omega_R^* \rho_0] + R_h - n_h/T_h(n_h - f_h)/\tau_h. \quad (4)$$

In Eq. (1), $\alpha = 2\pi\sigma/(\mu c)$ is the losses of a given electromagnetic mode with the refractive index μ , the non-resonant Ohmic conductivity of a sample at the optical frequency $\sigma(\omega)$, and the velocity of light in vacuum c . Γ is an overlap of the transverse distribution of the electromagnetic field with the MQW region. Here the amplitude of the polarization P is related to the amplitude of the off-diagonal element of the density matrix $\rho = \rho_0 e^{-i\omega t}$ for an electron and hole state with occupation numbers n_e and n_h and the dipole moment d of the optical transition as $P = (1/V)\sum_i d_i \rho_{0i}$, where the summation is over all electron-hole pairs on a given LL. Total volume densities are determined by a similar summation of n_e and n_h over the volume V of a structure. In Eq. (2), $\Delta = \omega_0 - \omega$ is the detuning of the frequency of the electromagnetic mode from the optical transition frequency

ω_0 and γ is the transverse decay rate. $R_{e,h}$ is the rate of influx of carriers from upper LLs and barriers; $T_{e,h}$ are total lifetimes of a given state due to radiative and non-radiative processes. The last terms in Eqs. (3) and (4) describe fast relaxation to quasi-equilibrium distributions $f_{e,h}$ with relevant time constant $\tau_{e,h}$ and Ω_R is the Rabi frequency of the electromagnetic mode²¹.

The optical transition frequency ω_0 , which determines Δ , is renormalized by screened Coulomb interaction with other carriers^{28,29}. This effect leads to a red-shift of the transition energy from its single-particle value $E_s = E_g + E_{e1} + E_{hh1} + (n + 1/2)\hbar eB/(m_r c)$, where n is the number of a given LL, E_{e1} and E_{hh1} are the edges of the ground subbands of electrons and heavy holes, and $1/m_r = 1/m_e + 1/m_{hh}$. For our structure $E_s \simeq 1.345 + 0.0023B(T)$ eV, where the magnetic field B is expressed in Tesla. By far the most important effect is the resonant interaction with electron-hole pairs on a given LL which defines both the growth rate of the instability and the polariton shift of the refractive index μ . In this regard, Γ is a crucial parameter in our gain-guided sample which strongly depends on the polariton contribution to the refractive index coming from excited carriers; see below.

The discrimination between SF and incoherent recombination regimes is convenient to formulate in terms of a linear initial-value problem, assuming initial quasi-equilibrium degenerate populations of carriers created by pumping and subsequent relaxation. After finding the linear susceptibility $\chi(\omega)$ from Eq. (2) one can solve the dispersion relation following from Eq. (1) and find the complex frequency $\omega(k)$ as a function of a real wave number k . Note that slow-varying amplitude approximation implies that $|\omega|$ and k are close to resonance frequency ω_0 and wave number $\mu\omega_0/c$. The instability, or exponential growth of the field and polarization with time, develops when $\text{Im}[\omega] > 0$. Obviously, for instability of any kind one needs positive population inversion $\Delta N \equiv n_e + n_h - 1 > 0$ with respect to stimulated recombination vs. absorption processes at the photon frequency.

Consider first an idealized situation when all scattering rates and transition frequencies are the same for all electron-hole pairs on a given LL, similarly to a homogeneously broadened active medium. Note that each spin-split LL has a degeneracy of $N_{2D} = eB/(2\pi\hbar c) \simeq 2.4 \times 10^{10} B(T) \text{ cm}^{-2}$, and total population inversion $\Delta N > 0$ can be defined as the difference between occupied and unoccupied states per unit area. In this case the dispersion relation $k^2 = \omega^2/c^2[\mu^2 + 4\pi i\sigma/\omega + 4\pi\chi(\omega)]$ has two solutions $\omega(k)$ – eigen modes that are sometimes called electromagnetic and polariton branches.

B. Emission Regimes and Growth Rates

The key parameter governing the instability of these modes and different regimes of recombination is the cooperative frequency ω_c that determines the coupling

strength between the field and the optical polarization as introduced in previous studies^{26,27,37}

$$\omega_c = \sqrt{\frac{16\pi^2 d^2 \Delta N \Gamma c}{\hbar \mu^2 \lambda L_{QW}}}. \quad (5)$$

Here L_{QW} is the total width of the QWs. When the inversion ΔN is small or negative, field oscillations decay with time and one can have only spontaneous recombination emission with power $\propto N_e/t_{sp}$ and characteristic timescale $t_{sp} \sim 1$ ns, where N_e can be presumed to be the same with the degeneracy in a LL in our experimental condition. The inversion can be increased by increasing the fluence of a pumping pulse and the magnetic field strength. With increasing inversion and optical confinement the modal gain may become higher than losses and oscillations of the field and polarization will grow with time. There are two basic regimes of the instability, depending on the ratio between the values of ω_c and incoherent relaxation times. They correspond to the instability of one of the two eigen modes existing in the medium. For low inversion density and fast decoherence, when $\omega_c \ll \gamma = 1/T_2$, one can have an amplified spontaneous emission (ASE) provided photon losses α are low enough. This is a regime of a one-pass amplifier, corresponding to the instability of the electromagnetic branch. Its growth rate

$$Im[\omega] = g_{ASE} \approx \frac{\omega_c^2 \gamma}{4(\gamma^2 + (k - k_0)^2)} - 1/T_E \ll \gamma \quad (6)$$

is much slower than the dephasing rate γ , where T_E is the photon transit time through the active region.

When the gain increases to the value such that $g_{ASE} L \mu / c \gg 1$, amplification proceeds in the saturated regime which is sometimes called superluminescence (SL). Here L is the length of an active medium in the propagation direction. The duration of the SL pulse in a saturated amplifier is $t_{SL} \sim L \mu / c$.²³

If there is feedback for any kind of modes existing in a sample, e.g., Fabry-Perot cavity modes formed by reflections from the edges, whispering gallery modes etc., then a system can lase on these modes. The growth rate of lasing modes will be defined by the same expression (6) with the optical confinement Γ and photon lifetime T_E defined for a given laser mode. One-pass amplification and lasing compete with each other and the process with a higher growth rate dominates. We argue below that there is no feedback and therefore no lasing for our samples, but it is important to stress here that *all* timescales for *all* of the above processes of ASE, SL, or lasing are longer than the dephasing time T_2 . Under such conditions the polariton mode is strongly damped with the decay rate γ and one can adiabatically eliminate optical polarization from Eqs. (1)-(4) assuming $\partial \rho_0 / \partial t = 0$ and $|\Delta| \ll \gamma$. The growth rate (6) has nothing to do with coherent dynamics of individual dipoles and originates from amplification of electromagnetic waves adiabatically followed by polarization.

Cooperative recombination regime (SF) results from the spontaneous formation of a large-amplitude coherent macroscopic polarization from initially incoherent oscillations of individual electron-hole dipole moments. It requires that $\omega_c > 2\gamma$, or $\omega_c > 2(\gamma\gamma^*)^{1/2}$ for a system with a large inhomogeneous broadening $\gamma^* \gg \gamma$ of frequencies ω_0 of electron-hole dipole oscillators^{10,26,27}.

When the field dissipation rate is very high, $\gamma < \omega_c/2 < 1/T_E$, cooperative emission develops with a growth rate $g_{SF} \approx \omega_c^2 T_E / 4 \propto \Delta N$. This instability of the polariton branch occurs *because of* Ohmic dissipation (the dissipative instability). However, it is not relevant for our samples that are characterized by a low field dissipation rate: $\omega_c/2 > \gamma > 1/T_E$. In this case the growth rate saturates at its maximum value $g_{SF} \approx \omega_c/2 \propto (\Delta N)^{1/2}$. Note that in all cases the SF growth rate is faster than the phase relaxation rate γ . This ensures maximally coherent nature of the process. In a sense, SF establishes an absolute upper limit on the rate with which an ensemble of initially incoherent inverted oscillators can radiate their stored energy.

The dynamics of SF is also noteworthy and very different from ASE or lasing. First, SF develops with a broad spectral bandwidth $g_{SF} > \gamma$ and thus cannot be described by usual rate equations based on adiabatic elimination of the polarization. Second, after the degenerate (inverted) population of carriers is established on a LL, the SF pulse is emitted with the delay time $t_d \sim (1/g_{SF}) \ln[I_{SF}/I_0]$ which is logarithmically larger than the inverse growth rate, where the logarithm factor of order 10-20 is due to the exponential growth of the field from the quantum noise level I_0 to the peak intensity I_{SF} . Third, the pulse duration $\tau_{SF} \sim 2/g_{SF}$ decreases with ΔN and therefore the pulse intensity $I_{SF} \sim N_e/\tau_{SF}$ scales superlinearly $\propto N_e^{3/2} \propto B^{3/2}$ with electron density or the magnetic field, assuming that $\Delta N \sim N_e$. The coherence length over which an individual pulse is formed is given by $L_c \sim ct_d/\mu$, which is a logarithmic factor of order 10 longer than the exponential amplification length $\sim c/(\mu g_{SF})$. Thus the volume of the active medium in which all electron-hole dipoles become phased and contribute coherently into an exponential amplification of a given electromagnetic mode is given by $\sim \Gamma \lambda^2 c / (\mu g_{SF})$. If we multiply it by the volume density of inverted oscillators $\Delta N / L_{QW}$ and by the spontaneous recombination rate of an individual e-h pair given by $1/t_{sp} = 32\pi^3 d^2 \mu / (\hbar \lambda^3)$, we obtain the maximum SF growth rate $\omega_c/2$ within a factor of 2.

The numerical value of the growth rate depends crucially on the optical confinement factor Γ . The contrast in the background refractive index $\Delta\mu \simeq 0.02$ between the MQW layer and GaAs is too low to provide wave guiding in a highly asymmetric waveguide formed by air on one side and GaAs on the other side of the MQWs. In the absence of a gain-induced change in the refractive index the modes are spread over the whole thickness of the sample and the overlap factor Γ is only $\sim 10^{-4}$ which rules out *all* stimulated amplification regimes, i.e., both

SF and ASE. Numerical simulations show that the minimum contrast needed for wave guiding is $\Delta\mu = 0.045$. The confinement factor Γ is 0.1 when $\Delta\mu = 0.05$ and reaches 0.4 with subsequent increase of the index contrast to 0.09 when $B = 25$ T. This affects the dependence of the ASE or SF growth rate and of the peak pulse power on the electron density or the magnetic field. Obviously the dependence becomes stronger, which can be directly observed in time-resolved measurements.

C. Gain Guiding

In an inverted medium the polariton contribution to the background refractive index is positive on the blue side of the transition frequency ω_0 , with the peak index change $\delta\mu \simeq \pi d^2 \Delta N / (\hbar \mu L_{QW} \gamma)$ reached at a detuning $\omega? \omega_0 \simeq \gamma$. For a high pumping fluence we can assume that all states are occupied and $\Delta N = 2N_{2D}$; then for $T_2 = 1/\gamma = 250$ fs $\delta\mu$ reaches the wave guiding threshold of 0.03 when $B \simeq 12$ T. The latter value corresponds to the experimentally observed appearance of the narrow stimulated emission peak on the blue side of the broad spontaneous emission spectrum; see Fig. 1.

Thus the polariton-supported wave guiding provides natural explanation of the observed blueshifted peak. If we adopt this explanation, then the observed stimulated emission threshold can be used to determine γ . The number we obtained supports the suggestion that the dephasing time for quantum-confined degenerate carriers on the LLs before the formation of the emission pulse can be as long as several hundreds fs. Unfortunately, this value of γ is difficult to verify independently, e.g. from the width of the spontaneous emission spectrum because γ may change significantly during one emission cycle due to varying density of carriers, and we collected only time-integrated data. Also, there could be some inhomogeneous broadening of the spontaneous emission due to sample inhomogeneity within the pumped spot. However, the width of the narrow stimulated emission peak does provide an additional information on the values of γ and the gain, which is consistent with the above estimate, as discussed below.

At the onset of wave guiding the stimulated recombination is still in the ASE regime, as discussed in more detail in Sec. 3A. The transition to SF occurs at $B \geq 20$ T, when the net growth rate $\omega_c/2 - \gamma/2 \simeq 8 \times 10^{12} \text{ s}^{-1}$ and $2N_{2D} \simeq 10^{12} \text{ cm}^{-2}$. The coherence length over which a SF pulse is formed is $L_c = ct_d/\mu \sim c/(\mu g_{SF}) \ln[I_{SF}/I_0]$. The ratio I_{SF}/I_0 is of the order of the total number N_t of e-h pairs contributing to a given pulse in the volume occupied by an electromagnetic mode, which we estimate as $N_t \sim 10^7$. Assuming $g_{SF} \sim \gamma \sim 4 \times 10^{12} \text{ s}^{-1}$, we obtain $L_c \sim 0.4$ mm. For observations of SF it is optimal to create an inverted (pumped) spot of this size. At much shorter lengths a SF pulse does not have time/distance to develop, while at longer distances $L \gg L_c$ independent SF pulses will be formed at segments of length L_c , creat-

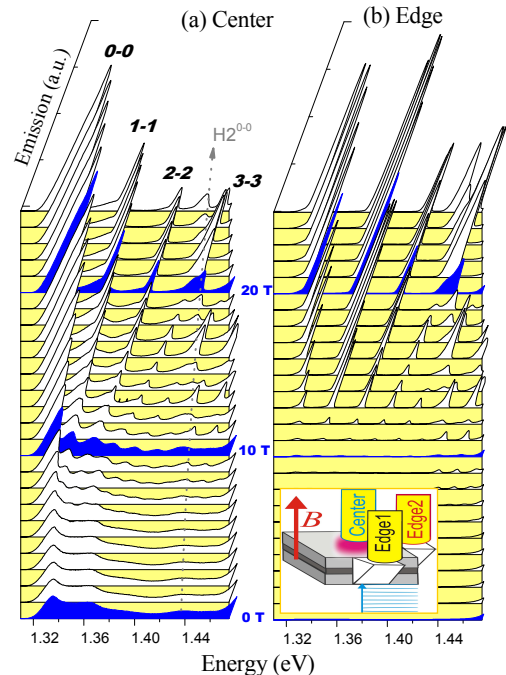


FIG. 1: (Color Online) Emission spectra as a function of magnetic field (a) for emission through sample above the excitation spot along the laser propagation direction and (b) for in-plane emission in an edge collection geometry. The inset of (b) shows the experimental schematic showing excitation pulses from the bottom and the collection fibers from the top. The pump fluence was 0.62 mJ/cm^2 . The gray dotted line denotes the position of the 0-0 LL of the e2-HH1 state.

ing a noisy output over the time interval $\sim L\mu/c$. Note that in a sample of the optimal pumped length L_c the shortest ASE pulse in a high gain regime has duration $\sim L_c\mu/c \sim 5$ ps, whereas a SF pulse is ≤ 1 ps.

After we defined all relevant spatial and temporal scales, let us turn to the experiments and their interpretation.

III. EXPERIMENTAL METHODS

Our experiments were performed in the new “Fast Optics” Facility at the National High Magnetic Experiments in Tallahassee, FL ³² using a 31 T DC Bitter magnet. $\text{In}_{0.2}\text{Ga}_{0.8}\text{As}/\text{GaAs}$ quantum well samples, consisting of 15 layers of 8 nm thick QWs separated by 15 nm GaAs barriers grown by molecular beam epitaxy, were used as samples. The magnetic field dependent low-power CW PL and absorption spectra of these samples are thoroughly described in Ref. 31. We used a 1 kHz repetition rate 775 nm or 800 nm Ti:Sapphire chirped pulse regenerative amplifier system to excite the sample. Both pulsewidth and fluence were varied to investigate scaling

laws. For reference, a pulse duration of 150 fs and pump fluence of $\sim 0.01 \text{ mJ/cm}^2$ generates a carrier density of $\sim 10^{12} \text{ cm}^{-2}$ in our samples.

The femtosecond excitation beam was delivered through free space into the magnet, and the plane of the QW was perpendicular to B with field up to 30 T. The emitted photoluminescence (PL) was collected using multimode optical fibers from the opposite face (center fiber) and cleaved edges of the sample (in the plane of the QW) using right-angle micro-prisms coupled to multi-mode optical fibers and analyzed with a high resolution MacPherson grating spectrometer equipped with a charge-coupled device (CCD) detector. The collection area of the prisms was $1 \times 1 \text{ mm}^2$, and the computed acceptance angle based in geometric considerations was $\sim 40^\circ$. Most of the spectra were collected by averaging the emission from approximately 1000 pulses; single pulse excitation using an external Pockels cell was used for excitation in experiments to probe the statistics of the directionality of the emission (Section IV C). Temperature-dependent spectra were collected from 10 K to 130 K to determine how dephasing effects influence the emission process. The pump spot size was varied in diameter as well as aspect ratio to examine the characteristics of the emission relative to the predicted coherence length of the electron-hole plasma.

IV. EXPERIMENTAL RESULTS AND FURTHER DISCUSSIONS

A. Dependence of Photoluminescence on Magnetic Field and Laser Fluence

Figure 1 displays emission spectra as a function of magnetic field B for a pump fluence of $\sim 0.62 \text{ mJ/cm}^2$ (a) from the opposite side of the sample above the pump spot (denoted by ‘center’; see inset) and (b) at the sample edge perpendicular to the excitation direction (‘edge’). The spectra in Fig. 1(a,b) both show well defined and broad ($\Delta E \sim 9 \text{ meV}$) LL states as reported in previous studies^{34,35}. However, at a threshold field $B = 13 \text{ T}$, narrow spectral features ($\Delta E \sim 2 \text{ meV}$) emerge from high-energy side of LL peaks. The narrow features grow rapidly and become dominant at higher B . Although clearly visible in both the center and edge geometries, the narrow emission features are generated with higher efficiency in the edge geometry; the integrated emission strength of the sharp feature in the 0-0 LL at 25 T is approximately 70 times stronger than the broad spontaneous emission.

To analyze the growth of the edge-collected signal with increasing B , the integrated strength from individual LLs was fitted using a Lorentzian lineshape analysis for the narrow blueshifted feature and a Gaussian lineshape for the broad low energy redshifted feature. A Gaussian lineshape is typical for spontaneous emission while a Lorentzian lineshape originates from homogeneously

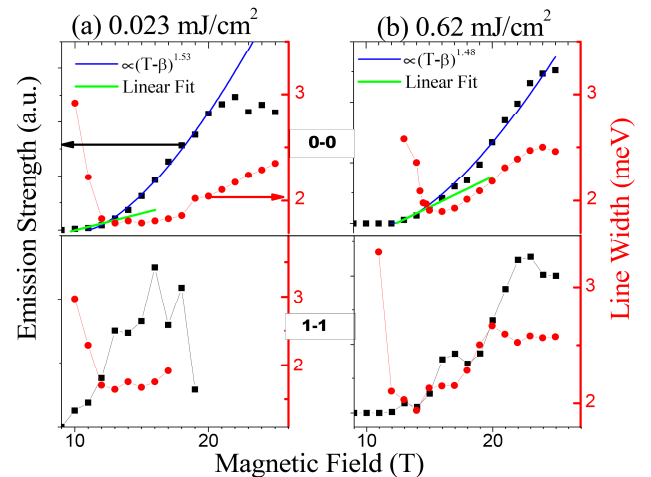


FIG. 2: (Color Online) Emission strength (black squares) and linewidth (red circles) of the narrow peak from 0-0 and 1-1 LLs versus B for different pump fluence of (a) 0.023 mJ/cm^2 and (b) 0.62 mJ/cm^2 . The blue and green lines represent the superlinear and linear scaling with B , respectively.

broadened systems. From the lineshape analysis, we obtained the integrated emission signal (black squares) and linewidth (red circles) traces in Fig. 2 for the pump fluence of (a) 0.023 mJ/cm^2 and (b) 0.62 mJ/cm^2 . At the lower fluence (Fig. 2(a)), the narrow emission 0-0 LL peak emerges at approximately 11 T, then increases as $\sim B^2$ until 20 T (indicated by dashed line). The linewidth undergoes a dramatic reduction (from 3 to $\sim 2 \text{ meV}$) as the field increases from 10 to 13 T, followed by a slow increase as the field is further increased. (Unless noted, we will refer only to the narrow emission feature in further discussions.) The 1-1 LL feature shows similar behavior with respect to threshold magnetic field and linewidth, although the integrated PL intensity grows linearly and begins to decrease at the highest field. The superlinear increase for the 0-0 emission in Fig. 2 (a) was accompanied by an sharp emission decrease from 1-1 LL, which indicates carrier depletion from higher to lower LL when the fluence of 0.023 mJ/cm^2 could barely saturate 0-0 LL.

At the higher fluence (Fig. 2(b)), the emission strength and linewidth display qualitatively similar behavior, however, the 1-1 LL emission oscillates substantially as a function of field. In addition, the increase in fluence allows for the emission from 0-0 and 1-1 LLs over the entire field range of 25 T. Below 11 T, narrow emission is not observed for any LL. In the case of 0-0 LL, the signal grows linearly with B from 12-14 T (green lines) and the linewidth reveals a significant correlation with the emission strength data. In the linear regime, the linewidth decreases monotonically versus B until the emission becomes superlinear, where the linewidth begins to increase.

To further investigate the origin of the oscillatory behavior with field, in Figure 3 we plot the emission

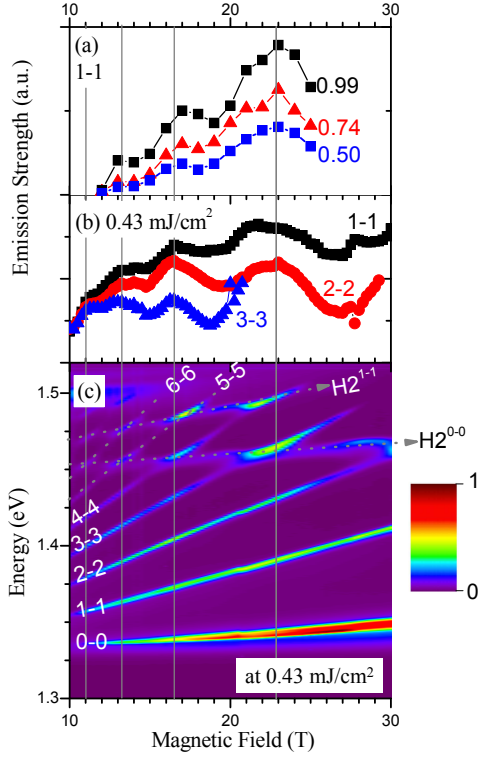


FIG. 3: (Color Online) Narrow line emission strength as a function of magnetic field from 10 - 30 T for (a) the 1-1 LL at various pump fluences and (b) 1-1, 2-2, and 3-3 LLs at a fixed pump fluence of 0.43 mJ/cm² obtained from a lineshape analysis of the emission data. In (c), we present a contour plot of the normalized emission strength versus field and energy for a fluence of 0.43 mJ/cm². The dashed gray lines in (c) show the mixing points between various LLs and higher sublevels, and the vertical lines show the correlation between the oscillation peaks and the mixing energies.

strength versus the magnetic field for the 1-1 LL at different fluences (Fig. 3(a)) and for different LLs at a fixed fluence (Fig. 3(b)). Above a fluence of 0.4 mJ/cm², the oscillations are a universal feature, independent of any specific LL or excitation fluence. For comparative purposes, a contour map of the field-dependent PL emission levels is presented in Fig. 3(c). In addition to the H1 LLs (labeled 0-0, 1-1, etc.), the higher heavy hole states H2⁰⁻⁰ and H2¹⁻¹ are observed (indicated by gray dashed lines) as reported in the previous study³¹. The gray vertical lines identify the mixing energies and the oscillation peaks: a clear correlation is seen between the mixing points of the H1-H2 levels and the peaks in the oscillations of the emission. At points where specific H1 and H2 LLs cross, a significant enhancement is seen in the emission strength of those LLs.

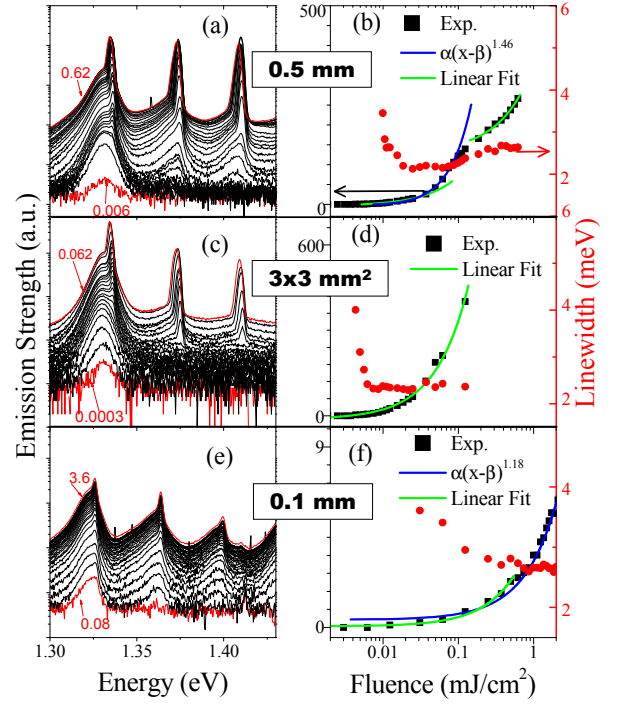


FIG. 4: (Color Online) Emission strength as a function of fluence at fixed field at 20 T for different spot sizes of (a) 0.5 mm diameter, (b) 3 mm and (c) 0.1 mm diameter. (d-f) Integrated emission intensity (black squares) and linewidth (red circles) of the narrow peak from the 0-0 LL versus fluence for different pump spot sizes. The fluence (x-axis) is plotted on a logarithmic scale. The inset of (a) shows the convolution method using a Lorentzian for the sharp peak and a Gaussian for the broader lower-energy peak. The blue (green) lines in (a-d) indicate the superlinear (linear) regime.

An observed spectral evolution of the PL emission as a function of e-h density from a broad spontaneous emission to a narrow peak on the blue side of the SE line, with subsequent further narrowing of the peak followed by its broadening is consistent with the scenario outlined in Sec. II. However, an observed spontaneous emission line has a full width of ~ 9 meV, larger than the homogeneous linewidth of 5 meV implied in the above discussion. The broad line may be caused by a variety of reasons, including time evolution of the emission spectrum due to changing density of carriers or spread of transition frequencies of e-h pairs. Assuming the latter, for an inhomogeneously broadened line, we calculated the numerically the growth rate and gain-induced index change of electromagnetic waves for a Gaussian profile of inhomogeneous broadening with full width $2\gamma^*$. Simulations

show that the index change of 0.03 corresponding to the onset of wave guiding for the same magnetic field of 12 T is achieved when $2\gamma^* \simeq 6$ meV and $2\gamma \simeq 3$ meV, i.e. it requires longer T_2 . In this case the total SE linewidth is $\simeq 9$ meV and the maximum index is reached at the blueshift $\simeq 5$ meV from the central frequency.

After the wave guiding is reached, the process enters a saturated SL regime accompanied by a line narrowing as a result of high-gain amplification. A diminishing linewidth is expected as the spectral components closest to the maximum of the gain spectrum get amplified stronger than components with greater detuning. An observed FWHM of the narrow peak changes with increasing e-h density from $2\gamma \simeq 5$ meV to $2\Delta\omega \simeq 2$ meV. If the maximum gain Eq. (6) at the center of the gain spectrum is equal to g_0 , it is easy to obtain the linewidth

$$\frac{\Delta\omega}{\gamma} = \left[\frac{g_0\mu/c}{\ln[(G_0 + 1)/2]} - 1 \right]^{1/2}, \quad (7)$$

Where $G_0 = \exp g_0 L\mu/c$. For $L = 0.5$ mm (the pump spot size), the observed narrowing by a factor of ~ 2.5 is consistent with the observed net amplification by a factor of order 100.

The transition to SF is accompanied by shortening of the pulse from $\tau_{ASE} \sim L\mu/c \approx 5$ ps to $\tau_{SF} \sim 4/\omega_c \leq 2/\sqrt{\gamma\gamma^*} \leq 1$ ps. This shortening of the pulse duration leads to the observed line broadening when the pulse duration becomes smaller than the inverse total bandwidth of the stimulated emission peak. If we identify $2\hbar/\tau_{SF} \sim \hbar g_{SF}$ with the observed emission full width of 2.5 meV at $B = 25$ T in Fig. 2(b), the value of the co-operative frequency is in the range 7–9 meV depending on the type of broadening we assume. This value is definitely higher than both $\hbar\gamma$ and $\hbar\sqrt{\gamma\gamma^*}$. Thus, spectral behavior is highly suggestive of a continuous evolution from a regime where ASE is the primary emission mechanism to an SF-dominated regime.

The intensity of a single SF pulse from a 0-0 LL scales with electron density N_e or the magnetic field B as $I_{SF} \sim \hbar\omega\Delta N/\tau_{SF} \propto N_e^{3/2}(\Gamma(N_e))^{1/2}$ or $B^{3/2}(\Gamma(B))^2$, where Γ is the overlap factor as introduced in Eq. (1).

assuming that the pump pulse fluence $J_p \propto \Delta N \propto N_e$. However, we cannot directly probe this superlinear scaling since the emission strength is integrated over 1s (1000 shots). Assuming all emitted photons are collected, we should observe a linear dependence of the integrated emission strength from N_e or B , which contradicts the observed superlinear dependence in the SF regime.

We interpret the superlinear scaling of time-integrated intensity of SF from 0-0 Landau level as the development of multiple SF pulses after each pumping shot. As the first SF pulse develops on the 0-0 LL and leads to a fast depletion of e-h pairs on this level on a sub-picosecond scale, e-h pairs on the 1-1 LL do not have time to recombine via a much slower ASE process. They lose energy relaxing to the 0th level and emit another SF pulse, leading to superlinear increase in the total fluence from 0th level.

There are several lines of evidence that suggest that. First, the superlinear scaling is observed only for the 0.5 mm spot, approximately the SF coherence length L_c as discussed in more detail above and in the next section; see Fig. 4. SF cannot develop for spot sizes smaller than the coherence length, whereas for larger spots many independent uncorrelated SF pulses are created, with the total emission resembling ASE rather than SF. Furthermore, the superlinear increase in the 0-0 LL emission is accompanied by a decrease in emission from higher LLs below 0.25 mJ/cm². Finally, the statistics of counts received by two edges in Fig. 6 is consistent with the formation of two pulses from the 0-0 LL, as explained in Section IV C.

At very high pump fluences, SF may develop from two or three LLs simultaneously, and the growth of the emission strength with the pump fluence and magnetic field should slow down.

B. Dependence of Photoluminescence on Excitation Area and Geometry

The characteristics of the emission can be influenced by the excitation spot size and by the geometry of the excitation region. A spot size that is comparable to the SF coherence length L_c is optimal for SF emission. A significantly larger spot size will excite densities over a large area result in a number of independently SF-emitting (and uncorrelated) regions of dimension on the order of L_c , while a smaller spot size will suppress the formation of SF. Figure 4 examines how the integrated signal and linewidth in the narrow emission peak varies with excitation area. For these data, the field was held fixed at 20 T and the fluence was varied from 0.006 to 2 mJ/cm². The left hand column displays the spectra (plotted logarithmically); the right hand column plots the integrated intensity and linewidth scaling. Figure 4(a,b) were obtained with spot size of 0.5 mm diameter, approximately equal to L_c for our conditions. In Fig. 4(b), we observe scaling behavior similar to field scaling of 0-0 LL as in Fig. 2(b), the integrated strength (black squares) evolves from a threshold of 0.01 mJ/cm² through a linear regime (green line; 0.01-0.03 mJ/cm²) to a superlinear regime (blue line; 0.03-0.2 mJ/cm²). Above 0.2 mJ/cm² in Fig. 3(b), the signal resumes a linear scaling after the SF from 0-0 LL is saturated as the level is fully filled. The sustained linear regime in the 0-0 LL is possibly associated with additional carriers passed on from higher LL in the later stage after the SF pulse burst. The carrier density which produces the linear scaling regime after saturation can only be sufficient for ASE but not for SF. Such carrier depletion from higher to lower LL was also manifested in Fig. 2 (a) via anti-correlation between 0-0 and 1-1 LL above 20 T. When the laser spot was increased (decreased) to 3 mm (0.1 mm diameter) as shown in Fig. 4(c,d) (Fig. 4(e,f)), qualitatively different behavior is seen. Narrow emission peaks were observed from each

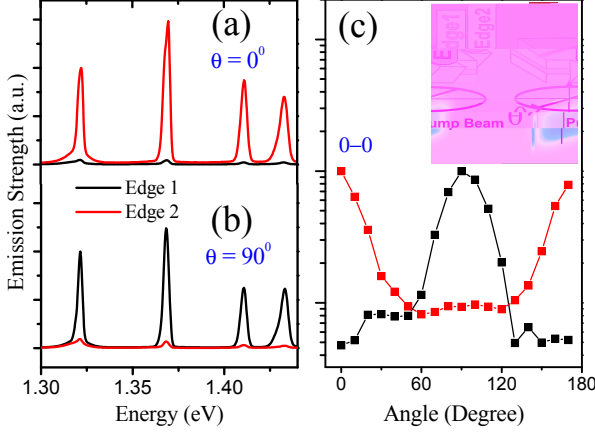


FIG. 5: (Color Online) Edge emission spectra measured from two orthogonally aligned fibers for the angle θ at a 0° and b 90° , where θ is the angular separation between the longer beam axis and the direction of edge 2 fiber as shown in the inset figure of c. In c, the emission strength of 0-0 LL is plotted for edge 1 (black) and edge 2 (red) as a function of angle.

LL, but both the integrated signal (black squares) and the linewidth (red circles) exhibits linear or nearly linear scaling, and in both of these cases the linewidth monotonically decreases with increasing fluence.

The shape of the excitation region can also be used to influence the emission characteristics. In particular, it is possible to control the SF emission orientation through tailoring the geometry of the gain region. Using a cylindrical lens to generate a rod-like 3 mm x 0.5 mm excitation region, Fig. 5 shows the output as a function of angle θ from 0° to 180° (see inset of Figure 5(c)) for a fluence $F_{laser} = 0.02 \text{ mJ/cm}^2$ and $B = 25 \text{ T}$. The maximum intensity follows the orientation of the long axis of the gain region. Tracing the output intensity displayed in Fig. 5(c) for edges 1 (black) and 2 (red), the emission is highly directional with a full-width-at-half-maximum of 40° . This value, comparable to the acceptance angle of our measurement, indicates the emission is highly directional. The variance in emitted power by 20 times between two directions are quite reasonable, since the gain should scale exponentially with propagation length, $e^{1.5/0.5} \sim 20$. Thus, the SF emission direction can be manipulated through tailoring of the gain geometry. However, this is not the unique feature of SF. The same behavior is expected from high-gain ASE. In addition, the increased signal of ~ 20 along the long axis relative to the short axis is due to exponential gain, as expected for a stimulated process.

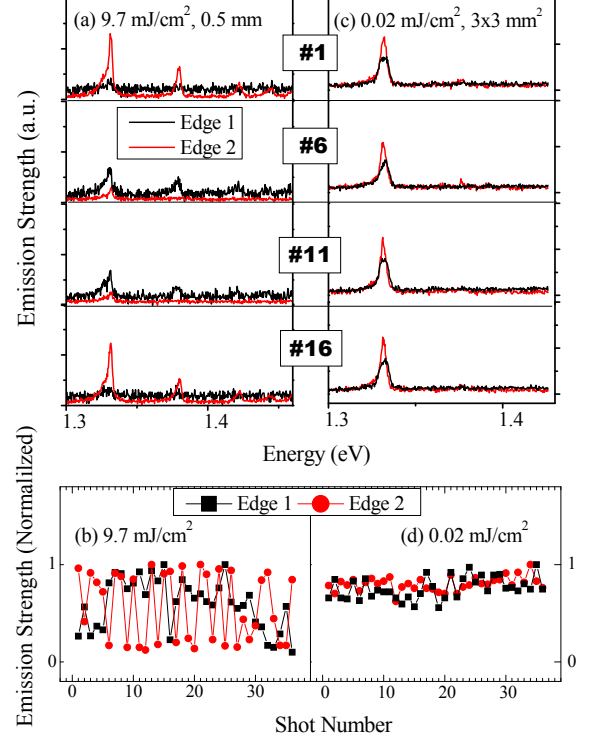


FIG. 6: (Color Online) Four representative emission spectra at 25 T from edge 1 (black) and edge 2 (red) fibers for (a) SF regime (9.7 mJ/cm^2 with 0.5 mm spot size) and for (b) ASE regime (fluence of 0.02 mJ/cm^2 and $3 \times 3 \text{ mm}^2$ spot size), excited from single laser pulse and measured simultaneously. Normalized emission strength from the 0th LL versus shot number in the (c) SF regime and the (d) ASE regime.

C. Stochastic Emission Characteristics

The strongest evidence for SF at high pumping fluences and magnetic fields in our samples comes from the random directionality experiment in the saturated SF regime ($> 0.2 \text{ mJ/cm}^2$). In this experiment, the pumped spot size was equal to one coherence length 0.5 mm, and radiation has been collected after single pulse excitation from two perpendicular edges simultaneously. Since the pumped area is a circle, both SE and ASE are emitted in all directions with the same intensity. This, however, is no longer true for SF. In the development of SF, initial quantum fluctuations grow to a macroscopic level and lead to strong fluctuations of the delay time from pulse to pulse. Initially, all propagation directions are equivalent. However, after one pulse has propagated in one direction, all e-h pairs are consumed along its path. Therefore, formation of the second pulse in the direction

traversing the path of the first pulse becomes suppressed. Indeed, a SF pulse consumes virtually all e-h pairs along its path leaving a narrow (of a few μm width) unpumped stripe with negative inversion ΔN . This stripe is *anti-guiding* for the blueshifted SF emission. This means that the SF radiation from any delayed pulse crossing the depleted stripe will spread over the whole thickness of the sample after just one wavelength $\lambda/\mu \sim 0.3 \mu\text{m}$ of propagation length. This reduces the overlap with an MQW layer to $\Gamma \sim 10^{-4}$, thus effectively quenching the pulse. Therefore, we should observe strong anti-correlation between the emission strengths received by the two edges after each pumping shot.

In order to verify this, we reduced the excitation pulse repetition rate down to 20 Hz and collected emission from two perpendicular edges whose outputs are mapped into spatially separate images in CCD detector.

Using a pump fluence of $9.7 \text{ mJ}/\text{cm}^2$ at 25 T, Fig. 4(a) illustrates typical spectra of SF after exciting one pump pulse, collected through edge 1 (black) and edge 2 (red) fibers for four representative shots, chosen from 36 shots in total. In Fig. 4(b), the outputs from edge 1 and edge 2 fibers were normalized to have the same maximum, although actual emission strength from edge 1 fiber was weaker, due to differences in the collection efficiency of each fiber.

We clearly observe that the two fiber outputs are anti-correlated over 19 different shots, which is about half of the total 36 shots. 16 events are those in which both edges receive significant radiation. There is only one event when both edges receive little radiation simultaneously. Over all of the shots, the maximum observed emission strength in Fig. 4(b) fluctuates as much as eight times the minimum value. This is far greater than the pump pulse fluctuation, on the order of a few percent, implying that each SF burst is very directional and randomly changing from pulse to pulse. The data can be best explained if there are two consecutive SF pulses that can be formed per each pump shot, according to the scenario suggested above. Each pulse can go either to edge 1 or to edge 2. Of course, there are also pulses generated in the opposite direction that we do not detect. At the same time, our collecting prisms are very wide ($1 \times 1 \text{ mm}^2$), so we collect most of the radiation propagating toward each of the two edges. Then in 50 % events both edges receive a SF pulse, or at least some radiation if there is not enough electrons for the second SF pulse and this second pulse is actually an ASE. In another 50 % events only one edge will receive both pulses.

At a lower $F_{\text{laser}} = 0.02 \text{ mJ}/\text{cm}^2$ (obtained with a $3 \times 3 \text{ mm}^2$ spot), qualitatively different behavior is seen; Fig. 6(b,d) shows omnidirectional emission on every shot, as expected for ASE or SE. At this much lower power with spot size much larger than the L_c , 1-1 LL is barely seen while higher LLs are not occupied.

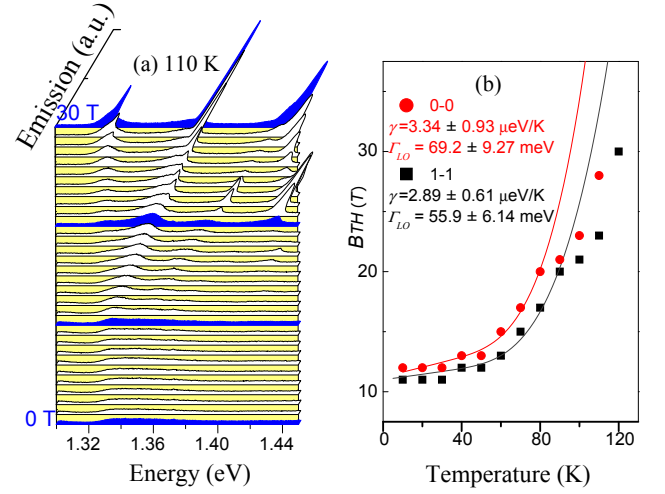


FIG. 7: (Color Online) Emission spectra at $T = 110 \text{ K}$ (b) The threshold field $B_{TH}(T)$ versus temperature (T) for the 0-0 LL (red circles) and for the 1-1 LL (black squares) sharp emission features as a function of temperature. The solid lines are fittings based on acoustic and optical phonon contributions from Eq. (2).

D. Dependence of Photoluminescence on Temperature

Because the formation of SF inherently relies on the establishment of a macroscopic coherence among the photoexcited carrier density, we expect that the emission threshold and strength should depend sensitively on temperature. An increasing phonon number with temperature should increase the intercarrier dephasing rate T_2 and thus increase the threshold magnetic field and carrier density. In Fig. 7 (a), we display the emission spectra obtained at a temperature of 110 K as a function of magnetic field. We observe sharp features from the 0th LL at a much higher magnetic field at $\sim 23 \text{ T}$. In addition, the sharp features tend to appear from higher LLs at lower fields with respect to the 0-0 LL as the field is increased. The sharp features, shortly appeared from 2-2 and 3-3 LLs in the 21-23 and 26-30 T range, is possibly associated with additional gain from increased density of state when overlapped with e-light-hole (for 2-2 LL) or with second confined level of e-heavy-hole (for 3-3 LL) transitions whose energy states are slightly renormalized compared to the case of low-power CW illuminations³¹. As we follow the threshold field $B_{TH}(T)$ for 0-0 LL (red circles) and for 1-1 LL (black squares) sharp feature in Fig. 5 (b), we observe it is more rapidly increasing above 50 K. Here, we define B_{TH} as the critical field for the appearance of narrow linewidth emission. Even though the B_{SF} is not coincident with B_{TH} since the sharp emission feature is generated by both the ASE and SF, we will presume their temperature variation is similar. First, note that the critical magnetic field B_{SF} for SF generation is obtained from relation between $\omega_c (\propto \sqrt{N})$ and the de-

phasing rate $2/T_2^{19,27}$, $\omega_c > 2/T_2$. The LLs density of states is given by $N = eB/h$, i.e., proportional to B and therefore to ω_c^2 . For electron-phonon scattering, the dephasing rate $2/T_2$ can be expressed phenomenologically as:

$$2/T_2 \propto \Gamma_0 + \gamma T + \Gamma_{LO}/[\exp(E_{LO}/k_B T) - 1], \quad (8)$$

where Γ_0 is the width due to the inhomogeneous broadening and γ (Γ_{LO}) is fitting parameter which measures the interaction with acoustic phonon (polar LO phonons). Thus, writing $eB_{SF}/h \propto \omega_c^2 = (2/T_2)^2$, we find

$$B_{SF} \propto (\Gamma_0 + \gamma T + \Gamma_{LO}/[\exp(E_{LO}/k_B T) - 1])^2, \quad (9)$$

Since the LO phonon energy E_{LO} in our sample structure, which is expected to be similar to that of GaAs-based QW (~ 36 meV), is much larger than thermal energy ($k_B T$) in our temperature range, we tentatively identify the acoustic phonon contribution as a dominant temperature mechanism for varying B_{SF} . The red (black) curve in Fig. 7(b) is the fitting based on Eq. (9) for 0-0 LL (1-1 LL), where we can obtain the comparative values of γ/Γ_0 and Γ_{LO}/Γ_0 , respectively. When Γ_0 being assumed to be the same with the minimum linewidth obtained from Fig. 2(b) ($=1.9$ meV), γ (Γ_{LO}) is smaller (larger) than that of 2-dimensional exciton case by 2-3 times (3-4 times)³⁹ while being very similar to the zero-dimensional case.⁴⁰ The deviation of the fitting curve above 80 K for 0-0 LL and above 90 K for 1-1 LL is possibly associated with carrier delocalization and/or deionized impurities at high temperatures.⁴¹ Γ_0 (~ 1.9 meV) indicates the SF pulse duration is shorter than 700 fs ($=2\hbar/\Gamma_0$) while the temperature dependence of $B_{TH}(T)$ agrees with the dephasing dynamics in zero-dimensional system.

E. Emission characteristics with stretched excitation pulse width

Finally, we investigate how the emissions depend on the excitation pulse width, as being compared with the delay time t_d . For the optimal coherence length L_c , t_d is roughly estimated around 10 ps when the pumping fluence of ~ 0.1 mJ/cm² almost saturates the available states in 0-0 LL (cf., Fig. 4(b)).³⁷ In this regard, in figure 8., the characteristics of the emission were examined with pulsewidth broadened up to 30 ps. The pulse stretcher was composed by a grating pair, a lens pair, and mirrors as cartooned in the inset of Fig. 8(a). The sample temperature and the laser fluence were fixed at 10 K and at around 0.1 mJ/cm² with which total excitation carrier density can reach $\sim 10^{13}$ /cm².

Fig. 8(a) shows corresponding emission spectra in the edge collection geometry with magnetic field from 0 to

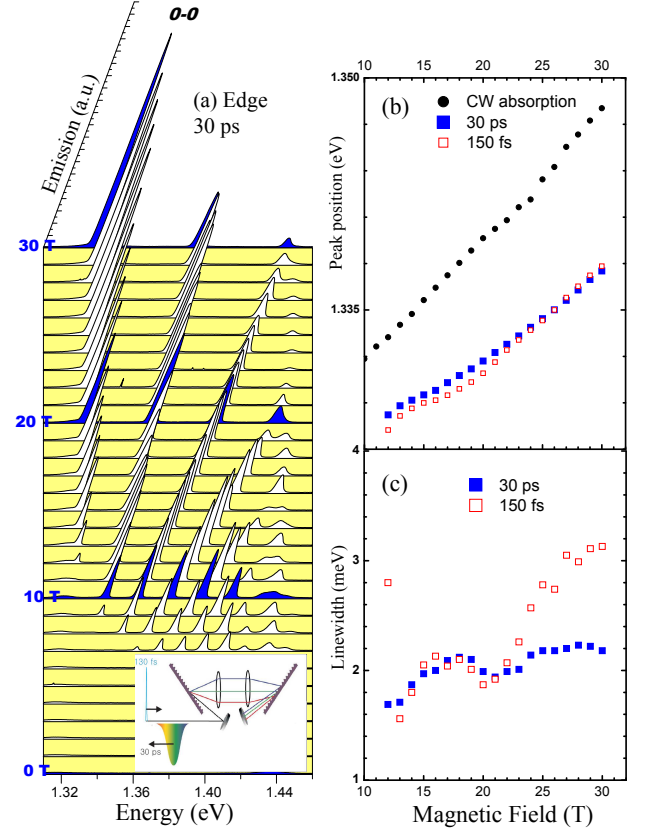


FIG. 8: (Color Online) (a) Emission spectra as a function of magnetic field for the excitation pulse width of 30 ps. The inset shows the pulse stretching scheme using two wavelength dispersing diffraction gratings. (b) 0-0 LL peak energy positions for the pulse width of 30 ps (solid square) and 150 fs (open square), compared with low power CW absorption. (c) Linewidth of the sharp feature from 0-0 LL versus B for 30 ps (solid square) and for 150 fs (open square).

30 T. The 1-1 LL emission strength, compared with 0-0 LL, was relatively much stronger than that of Fig. 1 (b). This indicates a certain amount of slow carrier relaxation from higher LL down to 0-0 LL exists in a temporal scale shorter than 30 ps. We also observe the evident oscillatory behavior at 1-1 and higher LLs which was introduced in Fig.3 with 150 fs pulsewidth excitation. In Fig. 8(b) we traced the peak energy positions of sharp Lorentzian feature in 0-0 LL at different excitation pulsewidths which were redshifted from previously studied case of Gaussian-fitted CW absorption³¹. The red-shifted peak position for pulsed excitation indicates not only the existence of localized states in these strained samples³¹ but also the band gap renormalization^{42,43}. We also note the effect of bandgap renormalization was stronger at 150 fs pulse but the difference between 150 fs and 30 ps was almost suppressed above 25 T. The 150 fs pulse creates carriers more abruptly than 30 ps pulse and the following carrier-carrier interactions will be enhanced

to screen the excitonic Coulomb interactions more effectively. The disappearance of the peak energy separation between 150 fs and 30 ps above 25 T, therefore, could be possibly associated with the combined effects of increased carrier density and reduced screening effects because of more strongly confined wavefunctions via B increment. The slope of peak position versus B in Fig. 8 (b) became more similar to CW absorption case with the increasing field, which suggests the reduction of effective mass renormalization in spite of increased carrier density at higher fields. More details on the field dependent variation of bandgap and effective mass renormalization will be discussed elsewhere.

To further characterize the emission in Fig. 8(c), we measured the linewidths for 150 fs and for 30 ps for Lorentzian sharp features in 0-0 LL. Fig. 8(c) displays the clear trend of increasing linewidths with B for 150 fs in contrast to those for 30 ps. As introduced earlier, 30 ps is much longer than the estimated delay time t_d to build coherence within L_c in our system and the intra-relaxation time on the order of 500 fs⁴². Since the increment of linewidth with B was a signature of SF, plateau in the linewidth trace for 30 ps in Fig. 8(c) implies the saturated amplified spontaneous emission, not reaching SF regime yet.

V. CONCLUSION

We have performed magneto-photoluminescence measurements in $\text{In}_x\text{Ga}_{1-x}\text{As}$ multiple quantum wells in high

magnetic fields using intense femtosecond pulses. The resulting density and energy confinement is sufficient to generate a spontaneous macroscopic polarization that decays through the emission of SF pulses. Our experiments demonstrate multiple evidence for the cooperative SF regime of spontaneous recombination as revealed by the spectral behavior, magnetic field and fluence scalings, spot size dependence, spatial and temporal correlations. We further probe the appropriate conditions for observing SF by exploiting its spectral features and dependence on the temperature and focal geometry.

Acknowledgments

This work was supported by the Korean Research Foundation Grant (MOEHRD, KRF-2007-313-C00218), the NSF ITR program (DMR-032547) and the Bio-imaging Research Center at GIST. A portion of this work was performed at the National High Magnetic Field Laboratory, supported by NSF Cooperative Agreement No. DMR-0084173 and by the State of Florida. A.B. acknowledges the support from the NSF CAREER program (0547019) and NSF PIRE and ERC programs.

-
- * Electronic address: jho@gist.ac.kr
- ¹ See, e.g., J. Shah, *Ultrafast Spectroscopy of Semiconductors and Semiconductor Nanostructures* (Springer-Verlag, Berlin, 1999).
 - ² Y. Yamamoto and A. Imamoglu, *Mesoscopic Quantum Optics*, (John Wiley & Sons, New York, 1999).
 - ³ S. T. Cundiff, A. Knorr, J. Feldmann, S. W. Koch, and E. O. Gobel, and H. Nickel, *Phys. Rev. Lett.* **73**, 1178 (1994).
 - ⁴ Tetsuji Tokihiro, Yoshihiro Manabe, and Eiichi Hanamura, *Phys. Rev. B* **51**, 007655 (1995).
 - ⁵ D. S. Jin, J. R. Ensher, M. R. Matthews, C. E. Wieman, and E. A. Cornell, *Phys. Rev. Lett.* **77**, 420 (1996).
 - ⁶ See, e.g., P. G. de Gennes, *Superconductivity of Metals and Alloys* (Benjamin, New York, 1966).
 - ⁷ M. Greiner, O. Mandel, T. Esslinger, T.W. Hansch and I. Bloch, *Nature* **415**, 39 (2002).
 - ⁸ L. V. Butov, A. C. Gossard, and D. S. Chemla, *Nature* **418**, 751 (2002).
 - ⁹ See, e.g., A.E. Siegman, *Lasers* (University Science Books, Sausalito, 1986), p. 549.
 - ¹⁰ V. V. Zheleznyakov, V. V. Kocharovskiy, and V. V. Kocharovskiy, *Sov. Phys. Usp.* **32**, 835 (1989).
 - ¹¹ R. Bonifacio and L. A. Lugiato, *Phys. Rev. A* **11**, 1507 (1975).
 - ¹² R. H. Dicke, *Phys. Rev.* **93**, 99 (1954).
 - ¹³ N. E. Rehler and J. H. Eberly, *Phys. Rev. A* **3**, 1735 (1971).
 - ¹⁴ N. Skribanowitz, I. P. Herman, J. C. MacGillivray, and M. S. Feld, *Phys. Rev. Lett.* **30**, 309 (1973).
 - ¹⁵ H. M. Gibbs, Q. H. F. Vrehen and H. M. J. Hikspoors, *Phys. Rev. Lett.* **39**, 547 (1977).
 - ¹⁶ R. Florian, L. O. Schwan, and D. Schmid, *Solid State Commun.* **42**, 55 (1982).
 - ¹⁷ P. V. Zinoviev, S.V. Lopina, Yu. V. Naboikin *et al.*, *Sov. Phys. JETP* **58**, 1129 (1983).
 - ¹⁸ M. S. Malcuit, Jeffery J. Maki, David J. Simkin, and Robert W. Boyd, *Phys. Rev. Lett.* **59**, 1189-1192 (1987).
 - ¹⁹ Y. D. Jho, X. Wang, J. Kono, D. H. Reitze, X. Wei, A. A. Belyanin, V. V. Kocharovskiy, V. V. Kocharovskiy, and G. S. Solomon, *Phys. Rev. Lett.* **96**, 237401 (2006).
 - ²⁰ M. Gross and S. Haroche, *Phys. Rep.* **93**, 301 (1982).
 - ²¹ Ω_R also contains non-resonant "local field" corrections from screened Coulomb interactions. We will however neglect them here, assuming $\Omega_R = dA/2\hbar$, where the dipole moment $d/e \simeq 0.5$ nm. The local field effect can be important for SF of a dense small sample of size much smaller than the wavelength. In our case it creates only a small correction to the SF dynamics.
 - ²² A. V. Andreev, V. I. Emelyanov and Yu. A. Ilyinskii, *Cooperative Effects in Optics* (IOP Publishing Ltd., Bristol, 1993).

- ²³ M. G. Benedict, A. M. Ermolaev, V. A. Malyshev, I. V. Sokolov, and E. D. Trifonov, *Superradiance. Multiatomic coherent emission* (IOP Publishing Ltd., Bristol, 1996).
- ²⁴ See e.g., D. Ammerlahn and J. Kuhl, B. Grote, S. W. Koch, G. Khitrova, and H. Gibbs, Phys. Rev. B **62**, 7350 (2000).
- ²⁵ A. A. Belyanin, V. V. Kocharovskiy, and V. V. Kocharovskiy, Solid State Commun. **80**, 243 (1991); Laser Physics **2**, 952 (1992).
- ²⁶ A. A. Belyanin, V. V. Kocharovskiy, and V. V. Kocharovskiy, Quantum Semiclass. Opt. **9**, 1 (1997).
- ²⁷ A. A. Belyanin, V. V. Kocharovskiy, and V. V. Kocharovskiy, Quantum Semiclass. Opt. **10**, L13 (1998).
- ²⁸ H. Haug and S. W. Koch, *Quantum Theory of the Optical and Electronic Properties of Semiconductors* (World Scientific, Singapore, 1994).
- ²⁹ M.W. Wu and H. Haug, Phys. Rev. B **58**, 13060 (1998).
- ³⁰ Although the very initial stage of SF requires full quantum electrodynamic analysis, the semiclassical approximation becomes valid as soon as the number of photons per mode becomes larger than one.
- ³¹ Y. D. Jho, F. V. Kyrychenko, J. Kono, X. Wei, S. A. Crooker, G. D. Sanders, D. H. Reitze, C. J. Stanton, and G. S. Solomon, Phys. Rev. B **72**, 045340 (2005).
- ³² <http://www.magnet.fsu.edu/usershub>
- ³³ G. Tränkle, H. Leier, A. Forchel, H. Haug, C. Ell, and G. Weimann, Phys. Rev. Lett. **58**, 419 (1987).
- ³⁴ L.V. Butov, V. D. Kulakovskii, E. Lach, A. Forchel, and D. Grutzmacher, Phys. Rev. B **44**, 10680 (1991).
- ³⁵ M. Potemski, J. C. Maan, K. Ploog, and G. Weimann,, Solid State Comm. **75**, 185 (1990).
- ³⁶ L.V. Butov, V. D. Kulakovskii, and A. Forchel, Phys. Rev. B **48**, 17933 (1993).
- ³⁷ A. A. Belyanin, et al., Laser Phys. **13**, 161 (2003).
- ³⁸ The high-field Landau notation is used to specify a QW electron-hole plasma in a magnetic field; for low-field—high-field correspondence, see, e.g., A. H. MacDonald and D. S. Ritchie, Phys. Rev. B **33**, 8336 (1986).
- ³⁹ H. Zhao, Sven Wachter, and Heinz Kalt, Phys. Rev. B **66**, 085337 (2002).
- ⁴⁰ I. Favero, G. Cassabois *, R. Ferreira, D. Darson, C. Voisin, J. Tignon, C. Delalande, G. Bastard, and Ph. Roussignol, and J. M. Gérard, Phys. Rev. B **68**, 233301 (2003).
- ⁴¹ J. Lee, E.S. Koteles, and M.O. Vassell, Phys. Rev. B **33**, 5512 (1986).
- ⁴² M.C. Tatham, J.F. Ryan, and C.T. Foxon, Phys. Rev. Lett. **63**, 1637 (1989).
- ⁴³ L. V. Butov, V. D. Egorov, V. D. Kulakovskii, and T. G. Anderson, Phys. Rev. B **46**, 15156 (1992).